IJE TRANSACTIONS C: Aspects Vol. 36 No. 06, (June 2023) 1066-1074

International Journal of Engineering

Journal Homepage: www.ije.ir

Numerical Modeling of Sediment-flow around Obstacle Inspired by Marine Sponges: Considering Body Configurations

M. Hashempour, M. Kolahdoozan*

Department of Civil and Environmental Engineering, Amirkabir University of Technology, Tehran, Iran

P A P E R I N F O

Paper history:
Received 19 December 2022
Received in revised form 27 March 2023
Accepted 31 March 2023

Keywords:
Synthetic Sponge
Sediment Concentration
Fluid Hydrodynamics
OpenFOAM
Marine Environment

A B S T R A C T

Coral reefs are exposed to extinction due to the sediment blocking through coral colonies. In this condition, there is no practical solution that originates from nature. Among all aquatic animals, marine tubular sponges have marvelous mechanisms. These natural creatures can inspire the design of a device for managing sediment-flow hydrodynamics. They suck flow from body perforation and pump water and undigested materials from the top outlet. Therefore, coinciding with receiving nutrients, the flow becomes circulated. This may help the momentum transfer through the coral colonies. In the current study, a synthetic sponge by motivating the tubular sponges was designed. Synthetic sponges' suction/pumping discharge was constant at 150 L/h. They have a body diameter of 8 and 15 cm and a height of 20 cm. The perforation area distribution changes to understand how it may influence sediment-flow hydrodynamics. The numerical modeling based on Reynolds Averaged Navier Stokes (RANS) equations and image processing technique (surface LIC) were deployed to determine the vortical flow patterns. Results confirmed that choosing the best body perforation configuration and area distribution can generate the dipole vortex. In this condition, a tornado combines with dipole and erodes the sediments to ≈ 30% near the bed. Moreover, the sediment concentration reduces to ≈ 20% in the water column at X/D =1. In this condition, it can be observed that the emergence of specific vorticities and re-circulations develops the suspension of particles. Therefore, the synthetic sponge with precise design can be practical for enhancing the momentum transferring and preventing pollutant blockage among coral colonies.

***doi**: 10.5829/ije.2023.36.06c.05*

NOMENCLATURE

$\vec{U}$	Mixture velocity	ρ	Mixture density (kg/m^3)
p	Pressure	α_m	Volume fraction of the mixture
g	Gravity (m/s^2)	α_1	Volume fraction of the air
S^*	Strain rate tensor	α_2	Volume fraction of the water
k	Turbulent kinetic energy per unit mass	α_3	Volume fraction of the sediment
I	Kronecker delta	μ	Mixture dynamic viscosity
D	Sponge body diameter	κ_{α_m}	Surface curvature of mixture
J	Sponge suction/pumping discharge (L/h)	σ	Surface tension
$\bar{C}_0$	Mean sediment concentration	τ	Reynolds stress tensor

1. INTRODUCTION

Coral reefs are the primary alive ocean ecosystems. They mainly exist in shallow waters and near the coasts. In this regard, they are prone to sedimentation and pollutant accumulation [1]. Human civilization operations, global warming, increasing water temperature, and wave height cause coral reefs to be exposed to extinction [2]. It is anticipated that 90% of coral reefs will be annihilated by 2040 [3].

*Corresponding Author Institutional Email: mklhdzan@aut.ac.ir
(M. Kolahdoozan)

Please cite this article as: M. Hashempour, M. Kolahdoozan, Numerical Modeling of Sediment-flow around Obstacle Inspired by Marine Sponges: Considering Body Configurations, ***International Journal of Engineering, Transactions C: Aspects***, Vol. 36, No. 06, (2023), 1066-1074

The coral reefs' death causes the migration of fishes and other aquatic animals, and then they will disappear forever due to losing their hometown and food resources. In addition, the extinction of the coral reefs causes harm to the coastlines and human residences via significant wave heights [1]. Various studies have focused on determining how corals influence flow and sediment hydrodynamics. A solution is expected to be provided for saving the coral reefs by learning from nature. Today it is believed that the branched corals' density is responsible for saturation velocity [4]. They stir the flow and enhance the momentum exchange to over 400% [5]. The passive vortices are in charge of the water stir phenomenon. They vanished where the loosely branched corals were presented [6]. An increase in turbulence directly influences the sedimentation/suspension rates of particles rear of the coral patch [7]. The reduction of velocity around corals causes sedimentation to be increased [8].

The tubular corals (sponges) also have interesting effects on flow hydrodynamics. A group called *Euplectella aspergillum* has mazed-helical ridges on the outer surface. This fabulous shape is the inspiration for engineering and structural designs. It totally suppresses the shedding behavior of Von-Karman street and moderates the uplift force. This leads to enhancing the sponge stability and preventing erosion of bed materials [9]. Removing the outer ridges causes the increase of vibration in the wake street due to the shear of the Boundary Layer (BL) [10]. The sponges suck flow from the body perforation (Ostia) and pump the water and undigested materials from the top outlet (Osculum). This function helps them to clean their residence, circulate flow, and receive nutrients without movement [11]. It may be interesting for controlling the sedimentation, nevertheless, the authors did not find any project or research that focuses on sponge planting for controlling sedimentation.

The yellow tube sponge (*Aplysina fistularis*) has a perforated-tubular shape. When it is lower than 20 cm, it has one column. By growing and reaching over 20 cm, it proliferates [12]. Figure 1 shows the yellow tube sponge compared to the *Staghorn coral* and *Giant barrel sponge* [13].

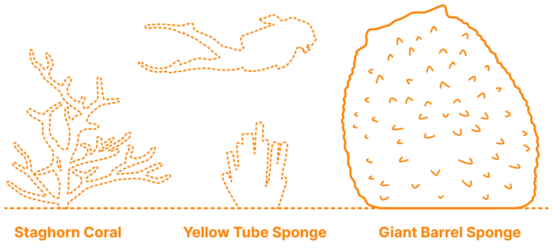

Figure 1. Yellow tube sponge versus Staghorn coral and Giant barrel sponge [13]

A singular tube of one cluster of yellow tube sponges has a 3-15 cm diameter. But a cluster diameter reaches up to 84 cm [14]. The body perforation has an average diameter of 270 μm [12, 15]. This sponge has various suction/pumping discharges within a day. The suction/pumping discharge varies with sponge size, pollutant/sediment concentration, water temperature, etc. [16, 17]. Figure 2, illustrates the yellow tube sponge dimensions [13, 14].

The innovation of the current study is inspiring the marine tubular sponges to design a new structure for enhancing the momentum transfer through the coral colonies. In this structure that will be called the *synthetic sponge* from now on, the physical shape and suction/pumping mechanism of natural tubular sponges were enthused. Numerical modeling was employed to investigate how the synthetic sponge can manage sediment-flow hydrodynamics and sediment concentration.

2. COMPUTATIONAL METHODS AND DETAILS

InterMixingFoam solver of OpenFOAM V.1812® was deployed for numerical modeling purposes. In continue, the details of the modeling, mesh generation, validation, and scenario preparation are presented.

2. 1. Basic Numerical Solution and Equations

The interMixingFoam solver is based on the Three-Fluid-Mixture (TFM) theory. Three phases (i.e., air, water, and sediment) are considered as fluids. The equations consist of phases concentrations and the relative velocity between water and sediment [18, 19].

$$\alpha_m = \alpha_2 + \alpha_3 \quad (1)$$

$$\alpha_1 = 1 - \alpha_m \quad (2)$$

where α_m, α_1, α_2, and α_3 are volume fractions of the mixture, air, water, and sediment, respectively. By using Reynolds Averaged Navier Stokes (RANS) equations, the governing equations of fluid flows (continuity and momentum) can be expressed as follows [20, 21]:

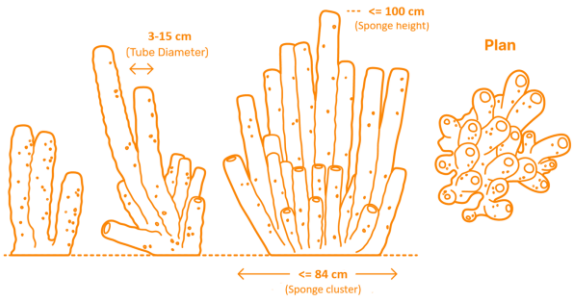

Figure 2. Yellow tube sponge dimensions [13, 14]

$$\nabla.\vec{U} = 0 \tag{3}$$

$$\frac{\partial \rho \vec{U}}{\partial t} + \nabla.\left(\rho \vec{U}\vec{U}\right) = \nabla.\left(\mu \nabla U + \rho \tau\right) - \nabla p + \rho g + \sigma \kappa_{\alpha_m} \nabla \alpha_m \tag{4}$$

where $\vec{U}$ is mixture velocity, p is pressure, ρ is mixture density, μ is mixture dynamic viscosity, g is gravitational acceleration, κ_{α_m} is surface curvature of the mixture, σ is surface tension [20], and τ is Reynolds stress tensor defined by the Boussinesq approximation as follows.

$$\tau = \frac{2}{\rho}\mu_t S^* - \frac{2}{3}k\delta \tag{5}$$

where μ_t is turbulent viscosity, S^* is strain rate tensor, k is turbulent kinetic energy per unit mass, and δ is Kronecker delta.

The two-equation of k-ω Shear Stress Transport (k-ωSSt) was deployed as a turbulence closure model. See the OpenFOAM manual for the details of the interMixingFOAM solver and k-ωSSt equations [22].

2. 2. Validation The Coleman [23] experiments were carried out for validation (Case No. 2). The 0.91 kg of sediment with a particle diameter of 105 mm was injected into a rectangular channel. The channel had 15 × 0.356 × 0.4 m (L× W× H) dimensions. Figure 3 shows the accuracy of the validation of velocity and concentration. The RMSE of concentrations and longitudinal velocities were 4.45E-5 and 0.0.069, respectively. Correlation coefficients between measured and computed data of concentrations and longitudinal velocities were 0.99 and 0.96 respectively. Therefore, the validation is acceptable.

2. 3. Model Setup Some scenarios were defined to investigate the effects of a synthetic sponge on sediment-flow hydrodynamics and concentration. The further details are as follows.

2. 3. 1. Synthetic Sponge The synthetic sponge has a perforated cylindrical shape that uses suction and pumping functions. The suction is done by body perforation, and the top outlet performs pumping. Figure 4 shows the synthetic sponge shape and mechanism versus the natural sponge. It is also worth to pay attention that the current study's goal is not simulating a natural tubular sponge. The main goal is to understand how a structure inspired by a tubular sponge influences sediment-flow hydrodynamics. The synthetic sponge has a larger perforation diameter and significant suction/pumping discharge compared to the natural one.

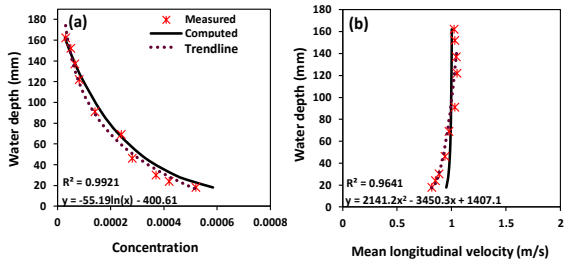

Figure 3. The accuracy of the numerical modeling: (a) concentration and (b) mean longitudinal velocity

2. 3. 2. Scenarios Five scenarios were designed to investigate the effects of synthetic sponges on sediment-flow hydrodynamics (Table 1). The perforation area distribution (the cumulative of the body pores area to the lateral area of the sponge) varies between 0.02-0.375. This range was chosen to facilitate the production of a synthetic sponge in the laboratory. In addition, since the body diameter of a single tube of the sponge has 0.03-0.15 m, the body diameter of the synthetic sponge (D) also was 0.08 and 0.15 m [25]. A natural sponge's height, when a single tube exists and before the emergence of branches, is less than 0.2 m [25]. Thus the synthetic sponge height (h) in all scenarios was 0.2 m.

The suction/pumping discharge of natural sponge also varies between 0.018-2.1 L/h [25]. Nevertheless, due to practical limitations, the suction/pumping discharge of synthetic sponge (J) was kept constant and equal to 150 L/h. The mean sediment concentration ($\bar{C}_0$) and velocity ($\vec{U}_0$) also were 0.000325 and 0.54 m/s, respectively. They

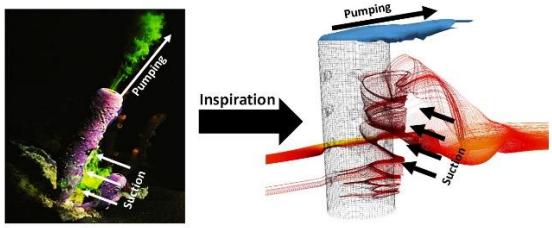

Figure 4. The natural tubular sponge [24] versus synthetic sponge

TABLE 1. Scenarios of the numerical study

Scenario	Perforation area distribution	Perforation diameter (m)	Body diameter (m)	Pores vertical distance (m)
M1	0	0	0.08	0
M2	0.0375	0.010	0.08	0.04
M3	0.0843	0.015	0.08	0.057
M4	0.375	0.010	0.08	0.015
M5	0.02	0.010	0.15	0.052

were chosen based on Coleman's [23] experiments about dilute sediment transport and Palau Salvador et al. [26] experiments, respectively.

2. 3. 3. Mesh Generation The channel has 2.32 × 0.356 × 0.4 m (L× W× H) dimensions. The sponge/rigid cylinder was located 0.32 m from upstream. The sponge was designed by CATIA V.5R21 software. The mesh generation also was prepared by SnappyHexMesh. The explicit surface and edge refinement levels were set to 1 and (0 2), and the unstructured boundary layer was set around the sponge. It is important to pay attention that the mesh sizes were selected based on the mesh independence analysis. Table 2 shows the mesh independence analysis. As can be observed, in the C3 scenario the percentage change is about 1 % and also has an acceptable size for capturing the vortices. Figure 5 shows the mesh and computational domain as well.

2. 3. 4. Boundary Conditions, Turbulence Model, and Solution Procedure The y^+ is the dimensionless quantity for the distance from the wall up to the center of the first grid cell. It is necessary to be checked to ensure the correct moddeling of the flow near the bed. When it comes to the near-wall treatment, three options exist:

TABLE 2. Mesh sensitivity analysis

Case No.	Mesh size (x × y × z) m	$\lvert\bar{U}\rvert$ (at X/D = 1)	$\left\lvert\frac{\lvert\bar{U}_{casei+1}\rvert-\lvert\bar{U}_{casei}\rvert}{\lvert\bar{U}_{casei}\rvert}\right\rvert\times100$
C0	0.013× 0.02× 0.016	0.2427	-
C1	0.026× 0.02× 0.008	0.2494	2.76
C2	0.026× 0.01× 0.016	0.2473	0.84
C3	0.013× 0.01× 0.008	0.2502	1.17
C4	0.0065× 0.01× 0.004	0.2809	12.25
C5	0.013× 0.005× 0.004	0.2980	6.07
C6	0.0065× 0.005× 0.008	0.2557	14.19

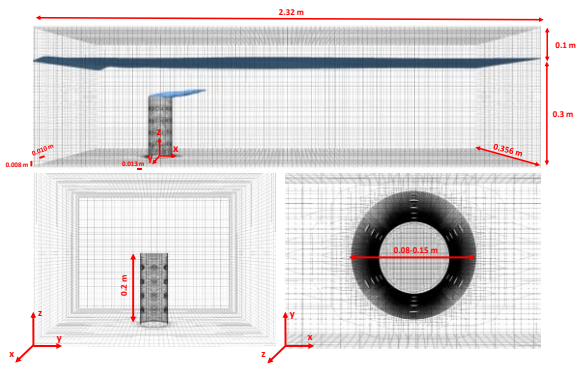

Figure 5. Computational domain and mesh structures

1. use wall function → $30 < y^+ < 300$
2. insensitive wall functions → $1 < y^+ < 300$
3. resolve the boundary layer → $y^+ < 6$

The use of wall functions allows using coarser grids [27]. In the current study, to prevent the computational cost and ensure the correct flow conditions, OpenFOAM special wall function was deployed. The y^+ parameter computes by the following equation [28]:

$$y^+ = \frac{y.u_\tau}{\upsilon} \quad (6)$$

where u_τ is the friction velocity, y is absolute distance from the wall, and υ is kinematic viscosity. The y^+ in the current study was between 30-200. Therefore, the OpenFOAM wall function provides desired accuracy. The velocity boundary conditions are defined in Table 3.

A K-ωSSt was used as a turbulence closure model. This model shows higher accuracy in detecting the flow separation downstream. k and ω coefficients were set to 0.11 and 0.85, respectively. The maximum CFL number, deltaT, and run-time also were 0.5, 0.001, and 80 seconds, respectively.

3. RESULTS AND DISCUSSION

In the current study, the Surface Line Integral Convolution (SurfaceLIC) was coupled with OpenFOAM. The SurfaceLIC is an image processing technique. It visualizes vector fields through the combination of noises and streaking (by black lines). However, additional image optimization is necessary to achieve the high accuracy of re-circulation zones [29]. In the current study, both LIC and color were used to enhance the contrast. Anti-aliasing (AA) was performed to prevent pixelation. A uniform noise texture was applied on flow sections to visualize the streaks of velocity vectors better. The noise texture and grain size were 128 and 2, respectively.

3. 1. The Surface Line Integral Convolution at Z/h= 0.25 Based on Figure 6, downstream of the rigid

TABLE 3. Velocity boundary conditions

Boundary	Velocity boundary condition
Channel inlet	fixedValue
Channel outlet	zeroGradient
Channel bottom	no-slip
Sponge/Cylinder wall	no-slip
Top of the channel	pressureInletOutletVelocity
Sponge perforation	flowRateInletVelocity (Discharge)
Sponge outlet	flowRateOutletVelocity (Velocity)

cylinder (M1 scenario), small re-circulation bubbles emerge. It is worth noting that the re-circulation bubble (re-circulation zone) consists of a stationary vortex, i.e., the vortex does not move. In this zone, the air core does not exist and the streamwise velocity component is negative. The bubbles are the erosive zones. The size of bubbles is less than when a rigid cylinder exposed the pure current. The presence of sediment causes energy extraction from the water. So the velocity and consequently, the size of the re-circulation bubble reduces. Another research also observed this for dense and dilute sediment-concentrated fluids [30]. The S marks in Figure 6, indicate the location of the bubbles' focies [31]. Focies were detected attached to the cylinder toe at X/D ≈ 0.51.

By replacing the rigid cylinder with the synthetic sponge, it was observed that whenever the perforation area and pores' vertical distance are small (M2 scenario), the streamlines do not separate in downstream. In this regard, the re-circulation bubble vanishes. In the M3 scenario, an asymmetric wake emerges by reducing the suction velocity. A primary wake bubble with a foci location of (X/D ≈ 0.8, Y/D ≈ -0.98) was detected near the sponge toe. The emergence of the primary bubble is due to the attaching of the shear layer rolling to the sponge's rear surface [31].

In the M4 scenario, a steady pattern generates when the perforation area distribution reaches 0.375. In this condition, two symmetric and counter-rotating re-circulation bubbles emerge downstream with core coordinates of (X/D ≈ 1.1, Y/D ≈ 1.1) and (X/D ≈ 1.1, Y/D ≈ -0.98). The generation of two recirculation bubbles can be due to the dipole generation, less sediment concentration in the water column, and flow suction by body perforation. In the M5 scenario, the conditions are nearly the same as in M2. But the sediment concentration downstream is much higher than in the M2 scenario. The reason will be discussed by vortical detection in future sections.

3. 2. The Surface Line Integral Convolution at Y/D = 0 For detecting the vertical concentration and flow hydrodynamics, image processing was deployed at a vertical surface in Y/D = 0 (Figure 7) downstream, a *quadrupole* vortex emerges. Its re-circulation core is at (X/D = 0.6, Z/h = 0.64). Since the sediment concentration near the bed is high, the up-wash and down-wash interact at a higher elevation. So a stagnation point (SP) emerges at (X/D = 0.9, Z/h ≈ 0.3). Meanwhile, for M2 and M3, the suction makes the *quadrupole* unstable and turns it into a *six-vortices type*. The *six-vortices type* was detected recently [32, 33]. It is a transitional condition between *dipole* and *quadrupole*. The *six-vortices pattern* can be identified by increasing the pores' vertical distance and diameter (Figure 7(c)). Nevertheless, a stagnation point occurs at (X/D = 0.7, Z/h = 0.47).

In the M4 scenario, the increase in a perforation area distribution reduces the concentration downstream of the sponge. Consequently, the downwash interacts upwash near the bed (Figure 7(d)).

Therefore, the six-vortices or quadrupole vanishes, and the dipole emerges. A dipole has the potential to generate a tornado (spiral) adjacent to the sponge. The suction via pores disturbs the downward flow pattern and consequently, a tornado occurs. In this condition, coinciding with the suction mechanism, a spiral pulls the sediment out from the bed. It transfers particles to higher water elevations, where the flow velocity is much more significant. Figure 8 is the 3D- modeling of streamlines which displays the *tornado* generation by sponge.

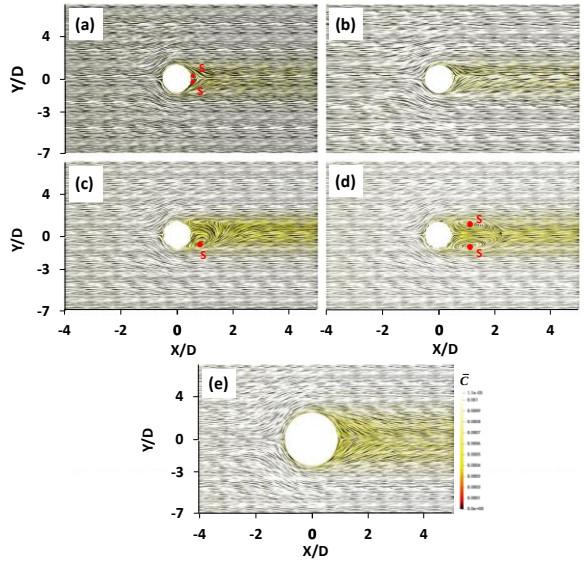

Figure 6. SurfaceLIC at Z/h = 0.25 for: (a) M1, (b) M2, (c) M3, (d) M4, and (e) M5

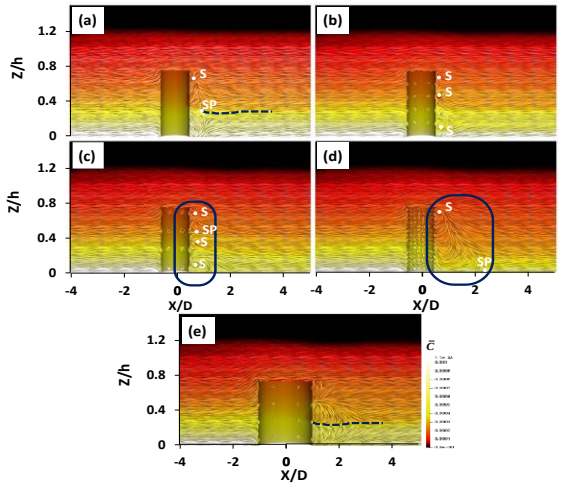

Figure 7. SurfaceLIC at Y/D = 0 for: (a) M1, (b) M2, (c) M3, (d) M4, and (e) M5

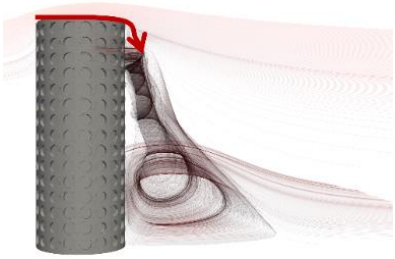

Figure 8. Tornado (Spiral) generation adjacent to the sponge in the M4 scenario

A similar tornado was observed downstream of a finite-height cylinder with H/D = 1.12 in low Reynolds number (Re_D = 16000) [32]. Nevertheless, the origin of the tornado is near the trailing edge of the synthetic sponge. Whereas, the origin of the tornado explained by Kirkil and Constantinescu [32] is near the bed. The difference in location is due to the cylinders' aspect ratios (AR) and relative boundary layer thickness (δ/h). The visualizations has been found by Zhang et al. [34]. However, due to using RANS modeling, the tornado's dimension can not accurately be captured.

Figure 9 confirms that at X/D = 1, the M4 scenario causes ≈ 20% reduction in sediment concentration compared to the M1 scenario (Figure 9(a)). In addition, it causes ≈ 11% and ≈ 30% sediment erosion compared to the rigid cylinder, at Z/h = 0.6 and Z/h = 0.2, respectively (Figures 9(b) and 9(c)). It is worth pointing out that herein *erosion* and *sedimentation* means sediment concentration decrease and increase, respectively.

In scenario M5, the suction effects become weak by reducing the pore area distribution to the lowest value among all scenarios. Therefore unique vortical patterns were not captured by surfaceLIC. As a result, a 2% increase in sediment concentration at X/D = 1 can be observed. Near the bed (Z/h = 0.2) and at Z/h = 0.6, the sediment concentration also is higher than when a rigid cylinder presents (≈ + 6%). Thus, it can be concluded that designing the perforation configuration and sponge body size is essential for managing the vortical flow and preventing sedimentation through the channel.

3. 3. The Surface Line Integral Convolution at X/D = 1

For understanding the sedimentation/erosion patterns, the surfaceLIC was deployed at X/D = 1. through a vertical surface (Figure 10).

In the M1 scenario, two clockwise and counter-clockwise patterns were detected. This was similarly detected in M2-M5 scenarios. They are known as Counter Rotating Vortex Pairs (CRVP). The CRVP generation makes an eroded ridge in the Y/D = 0. So the circulation pattern causes lateral sedimentation in the channel.

Besides, the extension of the horse-shoe vortex (EHV) legs can be identified on both sides of the rigid

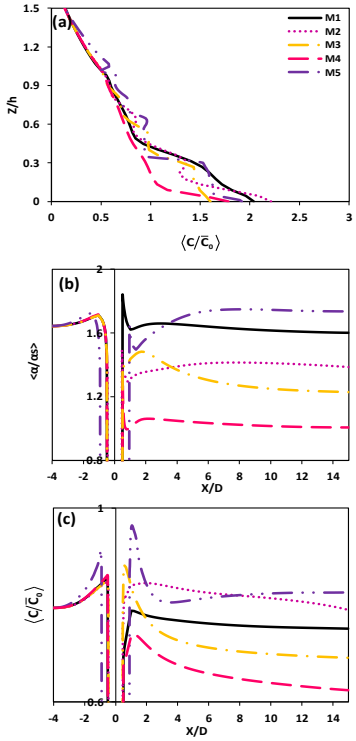

Figure 9. Concentration distribution at (a) X/D = 1, (b) Z/h = 0.2, and (c) Z/h = 0.6.

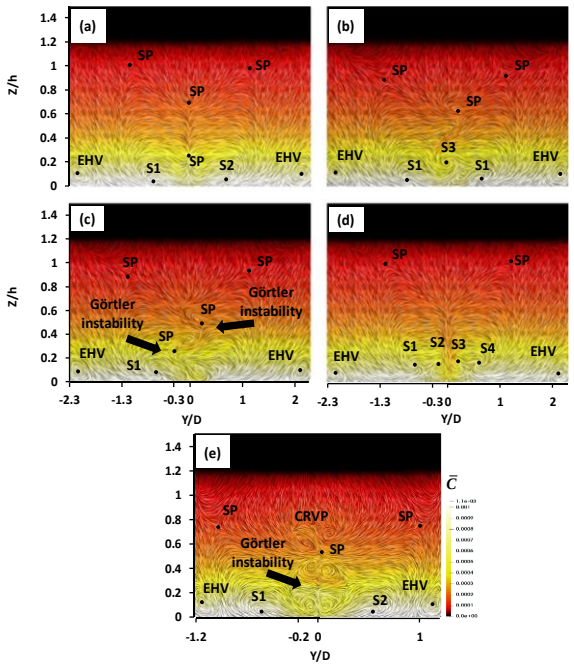

Figure 10. SurfaceLIC at X/D = 1 for: (a) M1, (b) M2, (c) M3, (d) M4, and (e) M5

cylinder/sponges. They are not precisely the downstream horse-shoe vortex or upstream vortices [35]. The horse-shoe vortex that continues downstream from the cylinder

helps sediment deposition in outer zones. In Figure 10(c), CRVP and similar mushroom vortex[1] can be detected. A mushroom vortex is often realized behind concave walls or along streamlines with a curvature form [36]. By reducing the perforation area distribution and pores'vertical distance (M5 scenario), the Görtler instability changes into the large dual mushrooms. The CRVP and the two-mushrooms generation disturb the sediment concentration and cause the suspended sediment through the water column. So, the results of Figure 9 were achieved.

It is also essential to pay attention that, based on Xu et al. [37], the pressure increase is the reason for changing the Görtler instability to completely round mushrooms. Nevertheless, Based on Figure 11, the place of perforations influences the fluid streamlines and the vortices generation. So, it is necessary to design the synthetic sponge's perforation configuration accurately to reach the best flow management.

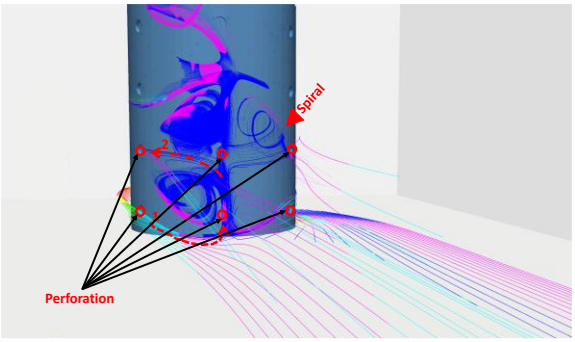

Figure 11. Streamline situations in the M5 scenario

4. CONCLUSION

In the current study, the marine tubular sponges were inspired to design a synthetic sponge. The synthetic sponge has a perforated tubular structure that sucks flow from the body perforation and pumps it from the top mouth. The numerical modeling based on RANS equations and image processing techniques were deployed to understand how synthetic sponges can influence sediment-flow hydrodynamics. Results confirmed that the perforation diameter, perforation area distribution, and perforation configuration influence the re-circulation bubble and vortices generation downstream of the sponge. The rigid cylinder causes quadrupole generation; meanwhile, sponges make it unstable. In this condition, regarding the sponge's characteristics *six-vortices* and a *dipole* generate.

The dipole and large tornado generation downstream of the sponge in the M4 scenario, reduce the sediment concentration to ≈ 20% in the water column. The CRVP production causes sedimentation in laterals and makes an eroded ridge in the middle of the channel.

Overall, it can be concluded that designing a device based on tubular sponges can influence sediment concentration through the water column. It can enhance sediment transport and momentum exchange. Therefore, the present design is anticipated to be practical for enhancing pollutant, sediment, and food transport through the coral colonies.

[1] Secondary Görtler Instability

5. ACKNOWLEDGMENT

This work was supported by the Iran National Science Foundation (INSF) [grant number 99018691].

6. REFERENCES

1. Woodroffe, C.D. and Webster, J.M., "Coral reefs and sea-level change", ***Marine Geology***, Vol. 352, (2014), 248-267. https://doi.org/10.1016/j.margeo.2013.12.006.
2. Fabricius, K.E., "Effects of terrestrial runoff on the ecology of corals and coral reefs: Review and synthesis", ***Marine Pollution Bulletin***, Vol. 50, No. 2, (2005), 125-146. https://doi.org/10.1016/j.marpolbul.2004.11.028.
3. Nace, T. *Nearly all coral reefs will disappear over the next 20 years, scientists say*. 2020; Available from: https://www.forbes.com/sites/trevornace/2020/02/24/70-90-percent-of-coral-reefs-will-disappear-over-the-next-20-years-scientists-say/?sh=5259cd1d7d87.
4. Jr, J. and Graus, R., "Water flow and hydromechanical adaptations of branched reef corals", ***Bulletin of Marine Science***, Vol. 25, (1975), 112-125.
5. Hossain, M.M. and Staples, A.E., "Passive vortical flows enhance mass transport in the interior of a coral colony", ***Physics of Fluids***, Vol. 31, No. 6, (2019), 061701. DOI: 10.1063/1.5094076.
6. Hossain, M.M. and Staples, A.E., "Mass transport and turbulent statistics within two branching coral colonies", ***Fluids***, Vol. 5, No. 3, (2020), 153. https://doi.org/10.3390/fluids5030153.
7. Folkard, A.M., "Hydrodynamics of model posidonia oceanica patches in shallow water", ***Limnology and Oceanography***, Vol. 50, No. 5, (2005), 1592-1600. https://doi.org/10.4319/lo.2005.50.5.1592.
8. Bartzke, G., Siemann, L., Büssing, R., Nardone, P., Koll, K., Hebbeln, D. and Huhn, K., "Investigating the prevailing hydrodynamics around a cold-water coral colony using a physical and a numerical approach", ***Frontiers in Marine Science***, Vol. 8, (2021). DOI: 10.3389/fmars.2021.663304.
9. Fernandes, M.C., Saadat, M., Cauchy-Dubois, P., Inamura, C., Sirota, T., Milliron, G., Haj-Hariri, H., Bertoldi, K. and Weaver, J.C., "Mechanical and hydrodynamic analyses of helical strake-like ridges in a glass sponge", ***Journal of The Royal Society Interface***, Vol. 18, No. 182, (2021), 20210559. https://doi.org/10.1098/rsif.2021.0559.
10. Quen, L.K., Abu, A., Kato, N., Muhamad, P., Tan, L.K. and Kang, H.S., "Performance of two- and three-start helical strakes in suppressing the vortex-induced vibration of a low mass ratio flexible cylinder", ***Ocean Engineering***, Vol. 166, (2018), 253-261. https://doi.org/10.1016/j.oceaneng.2018.08.008.

11. Region, P. and Leys, S.P., "Effects of sediment on glass sponges (porifera, hexactinellida) and projected effects on glass sponge reefs. (2013). *DFO Canadian Science Advisory Secretariat Research Document, 74*.
12. Rickborn, A.J., "The spatial ecology of a coral reef sponge, *Aplysina fistularis*." (2014). Ph.D. Dissertations, Boston University
13. Maddock, B. *Yellow tube sponge*. 2021; Available from: https://www.dimensions.com/.
14. Rickborn, A.J., "The spatial ecology of a coral reef sponge, *Aplysina fistularis*", Arizona State University, school of arts and sciences, Boston University, MA, (2010),
15. Machałowski, T., Rusak, A., Wiatrak, B., Haczkiewicz-Leśniak, K., Popiel, A., Jaroszewicz, J., Żak, A., Podhorska-Okołów, M. and Jesionowski, T., "Naturally formed chitinous skeleton isolated from the marine demosponge *Aplysina fistularis* as a 3d scaffold for tissue engineering", ***Materials***, Vol. 14, No. 11, (2021), 2992. https://doi.org/10.1016/j.carbpol.2021.118750.
16. Morganti, T.M., Ribes, M., Yahel, G. and Coma, R., "Size is the major determinant of pumping rates in marine sponges", ***Frontiers in Physiology***, Vol. 10, (2019), 1474-1474. DOI: 10.3389/fphys.2019.01474.
17. Strehlow, B., Jorgensen, D., Webster, N., Pineda, M.C. and Duckworth, A., "Using a thermistor flowmeter with attached video camera for monitoring sponge excurrent speed and oscular behaviour", ***PeerJournal***, Vol. 4, (2016). DOI: 10.7717/peerj.2761.
18. Ebtehaj, I., Azimi, H. and Bonakdari, H., "Numerical analysis of sediment transport in sewer pipe", ***International Journal of Engineering, Transactions B: Applications***, Vol. 28, No. 11, (2015),1564-1570. DOI:10.5829/idosi.ije.2015.28.11b.03.
19. Jafarmadar, s., "The effects of pressure difference in nozzle's two phase flow on the quality of exhaust mixture", ***International Journal of Engineering, Transactions B: Applications***, Vol. 26, No. 5, (2013), 553-562. DOI: 10.5829/idosi.ije.2013.26.05b.12.
20. Rodríguez-Ocampo, P., Ring, M., Fontes, J., Alcerreca-Huerta, J., Mendoza, E. and Silva, R., "Cfd simulations of multiphase flows: Interaction of miscible liquids with different temperatures", ***Water***, Vol. 12, (2020), 2581. DOI: 10.3390/w12092581.
21. Trimulyono, A., Chrismianto, D., Samuel, S. and Aslami, M.H., "Single-phase and two-phase smoothed particle hydrodynamics for sloshing in the low filling ratio of the prismatic tank", ***International Journal of Engineering,Transactions B: Applications***, Vol. 34, No. 5, (2021), 1345-1351. DOI: 10.5829/ije.2021.34.05b.30.
22. Ltd., O. *Openfoam manual*. 2022; Available from: https://www.openfoam.com/documentation/.
23. Coleman, N., "Effects of Suspended Sediment on the Open-Channel Velocity Distribution", ***Water Resources Research***, Vol. 22, No. 10, (1986) 1377-1384. https://doi.org/10.1029/WR022i010p01377
24. BIRD, J. *Sponges*. 2014; Available from: https://www.youtube.com/watch?v=m8a0oNsDEx8.
25. Hashempour, M. and Kolahdoozan, M., "Three-dimensional modeling of dilute sediment concentration around the synthetic sponge inspired by the tubular sponge mechanism", ***Ocean Engineering***, Vol. 271, 113799. https://doi.org/10.1016/j.oceaneng.2023.113799
26. Palau-Salvador, G., Stoesser, T., Fröhlich, J., Kappler, M., Rodi, W., "Large Eddy Simulations and Experiments of Flow Around Finite-Height Cylinders", ***Flow, Turbulence and Combustion***, Vol. 84, No. 2, (2009). DOI: 10.1007/s10494-009-9232-0
27 Introductory OpenFOAM® Course From 14th to 18th July, 2014. Wolf dynamics. University of Genoa, DICCA.
28. Jones, D., Chapuis, M., Liefvendahl, M., Norrison, D. and Widjaja, R., "Rans simulations using openfoam software., (2016).
29. Cabral, B. and Leedom, L.C., "Imaging vector fields using line integral convolution", in Proceedings of the 20th annual conference on Computer graphics and interactive techniques, Anaheim, Association for Computing Machinery., (1993 of Conference), 263-270.
30. Selim, T., Hesham, M. and Elkiki, M., "Effect of sediment transport on flow characteristics in non-prismatic compound channels", ***Ain Shams Engineering Journal***, Vol. 13, No. 6, (2022), 101771. https://doi.org/10.1016/j.asej.2022.101771.
31. Heidarinejad, G. and Delfani, S., "Direct numerical simulation of the wake flow behind a cylinder using random vortex method in medium to high reynolds numbers", ***International Journal of Engineering***, Vol. 13, No. 3, (2000), 33-50.
32. Kirkil, G. and Constantinescu, G., "Effects of cylinder reynolds number on the turbulent horseshoe vortex system and near wake of a surface-mounted circular cylinder", ***Physics of Fluids***, Vol. 27, No. 7, (2015), 075102. DOI: 10.1063/1.4923063.
33. Zhang, D., Cheng, L., An, H., Zhao, M., "Direct numerical simulation of flow around a surface-mounted finite square cylinder at low Reynolds numbers", ***Physics of Fluids***, Vol. 29, (2017), 045101. DOI: 10.1063/1.4979479.
34. Sumner, D., "Flow above the free end of a surface-mounted finite-height circular cylinder: A review", ***Journal of Fluids and Structures***, Vol. 43, (2013), 41-63. https://doi.org/10.1016/j.jfluidstructs.2013.08.007.
35. Sau, A., Hwang, R., Sheu, T. and Yang, W., "Interaction of trailing vortices in the wake of a wall-mounted rectangular cylinder", ***Physical Review E, Statistical, Nonlinear, and Soft Matter Physics***, Vol. 68, (2003), 056303. DOI: 10.1103/PhysRevE.68.056303.
36. Chen, Q., Yang, Z. and Wu, H., "Evolution of turbulent horseshoe vortex system in front of a vertical circular cylinder in open channel", ***Water***, Vol. 11, No. 10, (2019), 2079. DOI:10.3390/w11102079.
37. Xu, D., Liu, J., Wu, X., "Görtler vortices and streaks in boundary layer subject to pressure gradient: excitation by free stream vortical disturbances, nonlinear evolution and secondary instability", ***Journal of Fluid Mechanics***, Vol. 900, (2020). DOI: 10.1017/jfm.2020.438

Persian Abstract

چکیده

صخره‌های مرجانی به واسطه محبوس شدن ذرات رسوبی در بین کلونی‌های مرجانی مستعد انقراض هستند. در این شرایط راهکار عملی که خواستگاه آن از طبیعت باشد وجود ندارد. در میان تمام موجودات آبزی، اسفنج‌های دریایی لوله‌ای سازوکار خارق‌العاده‌ای دارند که می‌توانند برای مدیریت هیدرودینامیک جریان‌های رسوبی الهام بخش باشند. آن‌ها آب را از حفرات بدنه مکش کرده و سپس همراه با مواد غذایی جذب نشده از دهانه بالایی خود به درون ستون آب پمپاژ می‌کنند. در این فرآیند، همزمان با جذب مواد غذایی چرخش جریان نیز صورت می‌گیرد. در مطالعه حاضر، یک اسفنج مصنوعی با الهام گرفتن از اسفنج‌های دریایی استوانه‌ای طراحی شد. اسفنج مصنوعی ارائه شده دارای قابلیت مکش/پمپاژ با دبی ۱۵۰ لیتر بر ساعت بوده است. این اسفنج دارای قطر بدنه ۸ و ۱۵ سانتیمتر و ارتفاع ۲۰ سانتیمتر است. همچنین سطح توزیع حفرات در سناریوهای مختلف تغییر داده شد تا اثرات آن بر هیدرودینامیک جریان رسوبی بررسی شود. مدلسازی عددی بر پایه معادلات متوسط‌گیری شده زمانی به همراه پردازش تصویر جهت شناسایی جریان‌های گردابه‌ای بکار گرفته شد. نتایج نشان داد که انتخاب اندازه بدنه و نحوه آرایش حفرات روی آن می‌تواند منجر به شکل گیری یک گردابه دو قطبی شود. در این شرایط، گردابه دو قطبی با یک گرداب همراه شده که می‌تواهند غلظت رسوب را در نزدیک بستر تا ۳۰ درصد کاهش دهد. همچنین این اسفنج غلظت رسوب را در ستون آب و در مختصات X/D =1 به میزان ۲۰ درصد کاهش می‌دهد. در این شرایط، مشاهده گردید که تشکیل گردابه‌های منحصربفرد منجر به توسعه قابلیت تعلیق ذرات رسوبی می‌شود. بنابراین طراحی دقیق یک اسفنج مصنوعی می‌تواند برای بهبود انتقال مومنتوم و ممانعت از گیرافتادن ذرات در میان کلونی‌های مرجانی موثر باشد.